Chemistry–A European Journal
Research Article
doi.org/10.1002/chem.202403745
Chemistry Europe
European Chemical Societies Publishing
www.chemeurj.org

Scalable Bulk Synthesis of Phase-Pure γ-Sn_3N_4 as a Model for an Argon-Flow-Mediated Metathesis Reaction

Mirjam Zipkat,[a] Aylin Koldemir,[b] Theresa Block,[b] Claude Ceniza,[c] Teak D. Boyko,[d] Sebastian Kläger,[a] Reinhard M. Pritzl,[a] Alexander Moewes,[c] Rainer Pöttgen,[b] Stefan S. Rudel,*[a] and Wolfgang Schnick*[a]

Nitrides represent a promising class of materials for a variety of applications. However, bulk synthesis remains a challenging task due to the stability of the N_2 molecule. In this study, we introduce a simple and scalable approach for synthesizing nitride bulk materials. Moderate reaction temperatures are achieved by using reactive starting materials, slow and continuous mixing of the starting materials, and by dissipating heat generated during the reaction. The impact on the synthesis of using different starting materials as nitrogen source and the influence of a flux were examined. γ-Sn_3N_4 was selected as the model compound. The synthesis of pure γ-Sn_3N_4 bulk material on a large scale has still been a challenge, although a few synthesis methods were already described in the literature. Here we synthesized γ-Sn_3N_4 by metathesis reaction of argon-diluted $SnCl_4$ with Li_3N, Mg_3N_2 or Ca_3N_2 as nitrogen sources. Products were characterized by powder X-ray diffraction, scanning and transmission electron microscopy, energy-dispersive X-ray spectroscopy, dynamic flash combustion analysis, hot gas extraction analysis, X-ray photoelectron spectroscopy, Mössbauer spectroscopy and X-ray absorption and emission spectroscopy. Additionally, single-crystal diffraction data of γ-Sn_3N_4, previously unavailable, were successfully collected.

Introduction

During the last decades, interest in nitrides and their technological relevance has increased tremendously.[1] In 1993, years of optimizing the purity and crystal quality of gallium nitride (GaN) came to fruition with the successful commercial construction of the first efficient blue LED.[2] Nowadays, GaN and its solid solutions $Al_xGa_{1-x}N$ and $In_xGa_{1-x}N$ are amongst the most important materials for optoelectronic devices. Other nitrides, such as silicon nitride (Si_3N_4), are important non-oxide ceramics. Si_3N_4 features high fracture toughness, flexural strength, wear resistance and hardness as well as a low coefficient of thermal expansion and a low density.[3,4] In addition to nitrides that are already commercially used, there are many that feature or have been predicted to feature promising properties for solar energy conversion applications, such as photovoltaic, photoelectrochemical and photocatalytic devices, solid-state lighting, batteries, supercapacitors and more.[1,5–18]

Despite their promising properties, nitrides are still almost unexplored compared to oxides.[1,6,7] Reasons for this are synthetic challenges caused by the stable triple bond of the N_2 molecule (dissociation energy 941 kJ/mol) and the positive electron affinity of nitrogen (+0.07 eV).[6,19–21] Thermodynamically stable nitrides can be prepared by heating metals at high temperature in a nitrogen atmosphere.[22] However, nitrides have a large fraction of metastable phases.[23] Therefore, the majority of nitrides are susceptible to decomposition at high temperature. In order to avoid high temperature synthesis, nitrogen precursors that are higher in energy than N_2 can be used.[6,21,24] A large number of methods used for the synthesis of nitrides exploit this strategy. For example, common synthesis routes are ammonolysis, thermal decomposition of precursors and solid-state metathesis reactions.[21,25–32] Since metathesis reactions are typically very exothermic, high-pressure and solvothermal syntheses have proven to be effective.[13,31–35] High pressure shifts thermal decomposition to higher temperatures following Le Chatelier's principle. In solvothermal reactions, the solvent is absorbing heat produced during the reaction, leading to moderate temperatures. However, high-pressure methods lack scalability, while solvothermal reactions often result in impurities stemming from adsorbed or decomposed solvent. To provide more nitride materials for applications and to further investigate the structural and functional diversity of nitrides, development of new synthetic methods is required. Herein we introduce a straightforward, cost-effective and scalable approach for synthesizing nitride bulk materials, which is particularly suitable for thermally less stable nitrides. We achieve

[a] M. Zipkat, S. Kläger, R. M. Pritzl, S. S. Rudel, W. Schnick
Department of Chemistry, University of Munich (LMU), Butenandtstraße 5–13, (D) 81377 Munich, Germany
E-mail: stefan.rudel@cup.uni-muenchen.de
wolfgang.schnick@uni-muenchen.de
[b] A. Koldemir, T. Block, R. Pöttgen
Institut für Anorganische und Analytische Chemie, Universität Münster, Corrensstraße 30, 48149 Münster, Germany
[c] C. Ceniza, A. Moewes
Department of Physics and Engineering Physics, University of Saskatchewan, 116 Science Place, Saskatoon, Saskatchewan S7N SE2, Canada
[d] T. D. Boyko
Canadian Light Source, 44 Innovation Blvd, Saskatoon, Saskatchewan S7N SE2, Canada

Supporting information for this article is available on the WWW under https://doi.org/10.1002/chem.202403745

moderate temperatures by using reactive starting materials that are slowly merged in an argon flow, and by dissipating and absorbing the heat of reaction.

To demonstrate our novel synthesis method, metastable tin(IV) nitride, which adopts the spinel structure (γ-Sn_3N_4, space group $Fd\bar{3}m$) under ambient conditions, was chosen as the model compound.[36]

γ-Sn_3N_4 is a promising semiconductor material for various applications due to its direct band gap of $E_g = 1.6(2)$ eV and its high chemical stability.[15,36] Moreover, its composition of earth-abundant elements makes it an attractive option for technological development. γ-Sn_3N_4 has been reported to be suitable as a negative electrode material for sodium-ion batteries, exhibiting excellent gas sensing properties towards ethanol and being an efficient material for photoelectrochemical splitting of water.[12,13,37,38] Furthermore, γ-Sn_3N_4 has been predicted to have a free-exciton binding energy (D_e) of 69 meV and to have an estimated thermal-shock resistance of $H_V/\langle\gamma\rangle = 12$ GPa.[15,39] Both values exceed those of GaAs ($D_e = 4.2(2)$ eV, $H_V/\gamma_{th} < 8$ GPa), a semiconductor with similar electronic band gap that currently is a state-of-the-art material for IR-LEDs.[15,39,40]

First suggestions for the stability of Sn_3N_4 were reported in 1940.[41] Even so, the spinel structure of γ-Sn_3N_4 was not elucidated until 1999. Scotti *et al.* solved the structure using X-ray and neutron diffraction data.[36] They prepared microcrystalline γ-Sn_3N_4 in a two-step ammonolysis process. An imide-based intermediate was formed by reaction of a tin halide (SnI_4 or $SnBr_2$) with KNH_2 in liquid ammonia at −30 °C. After evaporation of NH_3, γ-Sn_3N_4 was obtained by thermal decomposition of the remaining intermediate at 300 °C. However, this synthesis method is methodologically complex and yields low amounts of the desired product. Large product loss occurs during the purification process and even after purification SnO_2 has been found in all samples.

Various other preparation routes have been developed for γ-Sn_3N_4, for both bulk and thin film form. Thin films can be obtained by reactive sputtering, which is most commonly used, and chemical vapor deposition.[38,42–49] Bulk γ-Sn_3N_4 can be synthesized via high-pressure solid-state metathesis, two-stage ammonolysis, a urea route or a metathesis reaction under solvothermal conditions.[12,13,37,50] The latter is relatively simple and easily scalable, but the products contain up to 12.4% carbon and 2.0% hydrogen caused by decomposition of the solvent.[13] Most recently, the synthesis of γ-Sn_3N_4 from the elements using a laser-heated diamond anvil cell (LH-DAC) was reported to achieve high purity, but the amount of sample is strongly limited.[39] Thus, the preparation of pure γ-Sn_3N_4 bulk material on a large scale remains a challenge.

Results and Discussion

Synthesis

In order to prevent products from decomposing due to the heat generated during exothermic reactions, it is necessary to ensure moderate temperatures during synthesis. The basic concept of the synthesis method presented in this work is to dilute a volatile halide with an inert carrier gas in order to limit the reaction rate of that halide with a reactive nitride. In addition, the carrier gas is dissipating the heat generated during the metathesis reaction. The reaction and crystallization can be enhanced by the use of a flux.

γ-Sn_3N_4 was synthesized via metathesis reaction of argon-diluted $SnCl_4$ with Li_3N, Mg_3N_2 or Ca_3N_2 according to Equations (1) and (2), respectively, with AE = Ca, Mg.

$$3\ SnCl_4 + 4\ Li_3N \rightarrow \gamma\text{-}Sn_3N_4 + 12\ LiCl \quad (1)$$

$$3\ SnCl_4 + 2\ AE_3N_2 \rightarrow \gamma\text{-}Sn_3N_4 + 6\ AECl_2 \quad (2)$$

$SnCl_4$ was used in excess (1.5 eq.) to ensure complete reaction of the nitride precursor.

The experimental setup is shown in Figure 1. For the synthesis, $SnCl_4$ was recondensed into the evaporator (B) and the nitride was placed on the frit (D) of the reactor (C, diameter: 2 cm). To perform experiments in a flux of molten tin, Li_3N, Mg_3N_2 or Ca_3N_2 were previously mixed with tin in an agate mortar.

The impact of various reaction parameters was examined, including temperature, argon flow rate and the ratio of tin flux to precursor. Since the experiments were carried out without a flow meter, comparisons between them are based on reaction time rather than argon flow rate. However, all experiments (with the same nitride starting material) used the same setup and quantity of $SnCl_4$, which was maintained at room temperature. As a result, the evaporation rate of $SnCl_4$ primarily depended on the argon flow rate. Each experiment was stopped immediately after the complete evaporation of $SnCl_4$, thereby directly linking the reaction time to the evaporation rate. A lower argon flow rate resulted in longer reaction times.

The temperature of the reactor was set within the range of 275 and 450 °C. Throughout those syntheses, a slow argon flow rate was maintained. All reactions were performed in a molten

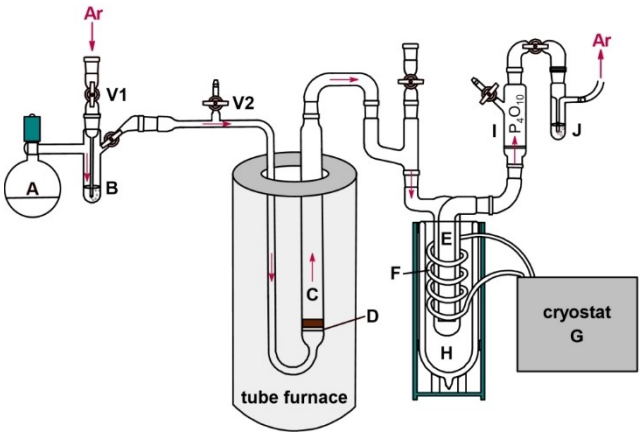

Figure 1. Experimental set up: (A) $SnCl_4$ storage flask, (B) evaporator with $SnCl_4$, (V1) valve for argon flow rate regulation, (V2) additional valve for argon flow rate regulation (C) reactor, (D) frit with Li_3N, Mg_3N_2 or Ca_3N_2 (and Sn), (E–I) waste-gas treatment: (E) cold trap, (F) copper coil, (G) cryostat, (H) dewar vessel with ethanol, (I) Sicapent® dry unit and (J) bubble counter.

tin flux. In order to investigate the impact of both, the argon flow rate and the tin flux, a series of experiments were carried out at 350 °C for Li_3N as precursor and at 325 °C for Mg_3N_2 and Ca_3N_2. All samples were washed with concentrated HCl(aq) and centrifuged, followed by washing with deionized water and absolute ethanol. Dark brown (micro)crystalline products were obtained. Following initial experiments that produced approximately 100 mg of product, yields were increased up to 1 g by optimizing the synthesis parameters and scaling up the batch size.

Parameter Optimization

Li-based nitrogen precursors have been proven to be suitable for synthesis of γ-Sn_3N_4.[12,13,50] Experiments were therefore first carried out using Li_3N as a starting material. The amount of tin flux, the argon flow rate and thus the reaction time and the reaction temperature were varied. PXRD patterns of the products are shown in Figure S2. Results of the Rietveld Refinements based on the PXRD patterns are shown in Figures S3–S5 and Tables S1 and S2. The Rietveld refinements yielded lattice parameters between 9.01351(20) and 9.04533(10) Å. In Table 1 the determined lattice parameters are compared to those reported in earlier works. All values are within the range of earlier reports.

Phase-pure (on the level of X-ray powder diffraction) γ-Sn_3N_4 was successfully synthesized within a temperature range from 275 to 400 °C. The presence of a tin flux does not appear to have an impact on the purity of the product. However, the use of a tin flux seems to improve the crystallinity of the product. The X-ray reflections of the sample synthesized without using a tin flux are slightly broadened compared to those of the products prepared in a tin flux (Figure S2a). Earlier reports already described that adding metallic tin significantly improves the crystallinity of γ-Sn_3N_4.[36]

The reaction time/argon flow rate has an impact on the position of the reflection maxima. Longer reaction times cause a slight shift towards smaller angles, which corresponds to increased lattice parameters (Figures S2b and S3). In addition, at extended reaction times (27 h), an asymmetric broadening of the reflections can be observed. The asymmetric broadening resulted in a smaller lattice parameter determined by Rietveld refinement. A possible explanation for increased lattice parameters is the progressive formation of nitrogen-deficient tin nitride due to incipient decomposition of γ-Sn_3N_4 as the reaction time increases. However, it should be noted that the shift of the reflections is minimal and no difference between the samples could be detected using other analytical methods. Possible causes for the asymmetric broadening are discussed below.

Table 1. Lattice parameters for γ-Sn_3N_4 obtained in this work and reported in literature.

a0/Å	Reference
9.0221(5)	this work (scXRD)
9.02458(3)	this work (PXRD PR: Mg_3N_2)
9.01351(20)–9.04533(10)	this work (PXRD PR: Li_3N)
9.037(3)	N. Scotti *et al.*[36]
9.0144(1)	M. P. Shemkunas *et al.*[50]
9.03716(5)	X. Li *et al.*[12]
9.0549(2) 9.0514(4) and 9.139(2)	S.D.S. Fitch *et al.*[13]
9.0187(5)	A. Zerr *et al.*[39]

The most evident influence of a molten tin flux and the reaction time concerns the yield (Figure 2). Long reaction times and the presence of a tin flux lead to yields of up to 54 %. The highest yield for experiments without added tin was 29 %. Short reaction times lead to maximal yields of 16 %. In scaling experiments conducted in this study, the batch size had no effect on the relative yield. The tin melt supposedly counteracts decomposition of γ-Sn_3N_4 during synthesis by absorbing the heat generated during reaction. In addition, the reaction is likely being facilitated by enhanced diffusion. Liquid tin with its excellent wettability has already been shown to be an appropriate flux for the synthesis of (poly)phosphides, arsenides and antimonides.[51] The influence of the reaction time and thus the argon flow rate is most likely attributed to the fact that using a lower argon flow rate at a constant $SnCl_4$ temperature and thus constant vapor pressure, results in less reaction heat per time, as the starting materials are merged more slowly. This enables better dissipation of the reaction heat and consequently, less γ-Sn_3N_4 decomposes during synthesis. In principle, the used reactor allows for the separation of argon flow rate and $SnCl_4$ evaporation rate by adding a second argon stream via the additional valve (V2). Thus, heat dissipation could be enhanced with a high auxiliary argon flow, while maintaining a low $SnCl_4$ evaporation rate, but this option was neglected so far.

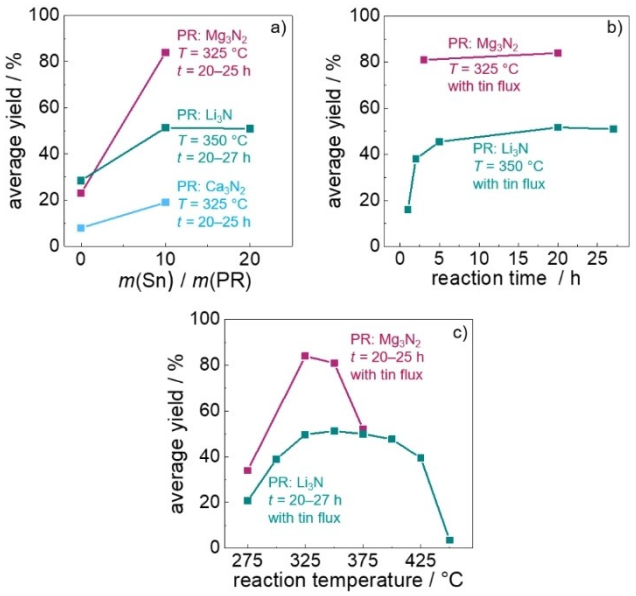

Figure 2. γ-Sn_3N_4 yields from reactions of $SnCl_4$ with Li_3N, Mg_3N_2 or Ca_3N_2 (PR denotes the precursor for the reaction) depending on the a) amount of tin, b) reaction time and c) reaction temperature.

Comparing the PXRD patterns of the products prepared at different reaction temperatures (Figure S2c), a reflection broadening and a shift towards smaller 2θ values is observed with increasing reaction temperature for $275\,°C \leq T \leq 350\,°C$. The broadening of the reflections indicates that the γ-Sn_3N_4 samples prepared at lower temperature exhibit better crystallinity than those prepared at higher temperatures. The shift of the reflections, and thus the increase of the lattice parameter (Figure S3), may be attributed to the formation of nitrogen-deficient γ-Sn_3N_4, as previously discussed. Similar to the samples prepared with varying reaction times, no differences were detected between the samples using other analytical techniques. At 375 °C, an asymmetric broadening of reflections appears at higher 2θ values, resulting in a smaller lattice parameter obtained by the Rietveld refinement (Figure S3). For the product obtained at 400 °C, the asymmetric broadening is less pronounced than for the product obtained at 375 °C. However, this difference is likely due to the fact that the reaction time for the 375 °C synthesis was 27 hours, whereas the 400 °C synthesis had a shorter reaction time of only 20 hours. As noted above, extended reaction times also result in asymmetric broadening of the reflections. Previous reports on γ-Sn_3N_4 explain the asymmetric broadening feature by the fact that the sample consists of a mixture of nano-sized and larger crystallites.[13] However, the PXRD pattern of the product prepared at 425 °C shows a splitting of the reflections at higher angles, which indicates that the asymmetric broadening is more likely caused by the formation of two or more tin nitride phases. In general, a splitting of reflections can either be attributed to the fact that two (or more) tin nitride phases with different lattice parameters have been formed, or to a distortion of the structure and an associated loss of symmetry. The lack of splitting of the reflections of the product prepared at 450 °C suggests that at least two tin nitride phases with different lattice parameters were formed at 425 °C. The reflections of the tin nitride, which was obtained at 450 °C, are significantly shifted to higher 2θ values. In addition, a substantial formation of SnO_2 occurred. Thus, the formation of more than one phase and the shift to higher 2θ values is most likely due to O_N substitutional defects. We attribute the presence of oxygen to the fact that the reactor, which is made of glass, is affected considerably by lithium at higher temperatures. To avoid this problem, we carried out further experiments using other nitrides as starting materials (Mg_3N_2, Ca_3N_2). Lithium nitride, used as the starting material, has been excluded as a significant oxygen source. The analyses performed show no evidence of oxide, suboxide, oxynitride or hydroxide impurities (Figures S8, S9 and Table S4).

Experiments using Ca_3N_2 (Figures S8, S10 and Table S4) as the starting material at 325 °C with and without tin flux yielded microcrystalline γ-Sn_3N_4 (Figure S6). The crystallinity and the yield, however, were worse than with Li_3N as a starting material. A maximal yield of 19% was obtained. It should be noted that the nitrogen content of the Ca_3N_2 used as the starting material was 34 at-%, which is lower than the theoretical value of 40 at-%, indicating the presence of impurities in the starting material.

In contrast, the use of Mg_3N_2 (Figures S8, S11 and Table S4) as a nitrogen-containing precursor resulted in phase-pure γ-Sn_3N_4 (on the level of X-ray powder diffraction) with sharper reflection profiles, indicating larger crystallites compared to the products obtained from the reaction with Li_3N. Figure S7 illustrates the PXRD patterns. Unlike the PXRD patterns described above, no shift or asymmetric broadening of the reflections is observed for different reaction times or temperatures. Based on the PXRD pattern of the sample synthesized at 325 °C a Rietveld refinement was carried out (Figure 3). The crystallographic data of the Rietveld refinement can be found in Table S3. The Rietveld refinement yielded a lattice parameter of 9.02458(3) Å.

In addition to enhanced crystallinity, the synthesis of γ-Sn_3N_4 via the Mg_3N_2 route also achieved higher yields (Figure 2). Using a tin flux, yields of up to 82% were obtained at 325 °C, ~30% more than when Li_3N was used as the starting material and ~60% more than when Ca_3N_2 was used.

The observation that Mg_3N_2 is more suitable for the synthesis of nitrides, which decompose at elevated temperatures, than Ca_3N_2 and Li_3N has been previously described for the synthesis of Mn_3N_2.[52] This was attributed to the fact that the reaction of $MnCl_2$ with Mg_3N_2 is less exergonic than the reaction of $MnCl_2$ with Li_3N or Ca_3N_2 and to the solid solution behavior of $MnCl_2$ and $MgCl_2$. For LiCl and $MnCl_2$ as well as $CaCl_2$ and $MnCl_2$ no formation of a solid solution was observed. The authors also mentioned that the more covalent character of Mg_3N_2 compared to Ca_3N_2 could kinetically inhibit the formation of N_2.

However, syntheses with Mg_3N_2 without a tin flux resulted in a yield of only 23%. This is lower than the yield obtained when employing Li_3N (yield: 28%). Nevertheless, the crystallinity of the product prepared with Mg_3N_2 was better. The aforementioned reasons as to why Mg_3N_2 is more suitable for synthesis therefore appear to apply only to a limited extent in this case.

A possible explanation for the significant improvement in both yield and crystallinity for the synthesis of γ-Sn_3N_4 with Mg_3N_2 with the addition of tin compared to the other routes is

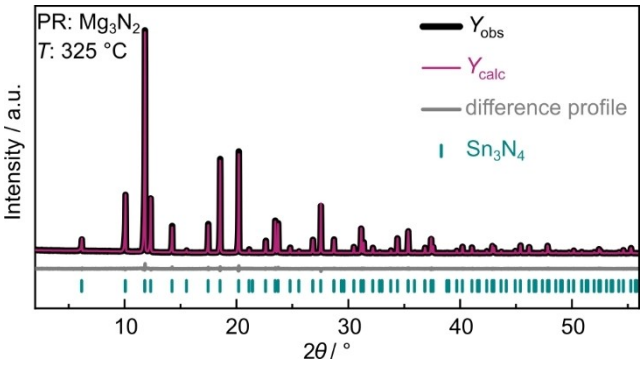

Figure 3. Rietveld refinement based on powder XRD data of γ-Sn_3N_4 prepared at 325 °C from the reaction of $SnCl_4$ with Mg_3N_2 in a tin flux, with experimental data (black line), calculated diffraction pattern (magenta line), difference curve (gray line) and positions of Bragg reflections of γ-Sn_3N_4 (vertical turquoise bars). The pattern was collected with Ag-Kα_1 radiation ($\lambda = 0.55954$ Å) in para-focusing Debye-Scherrer geometry. The refinement resulted in $R_p = 4.05$, $R_{wp} = 5.71$, $R_{exp} = 4.33$, $R_{Bragg} = 1.25$ and $X^2 = 1.32$.

most likely that Mg_3N_2 (or an intermediate) has better solubility in tin than Li_3N or Ca_3N_2. Consequently, the positive effect of the flux is more pronounced in the Mg_3N_2-using synthesis. Unfortunately, we could not find any reports on the solubility of Mg_3N_2, Li_3N or Ca_3N_2 in tin.

Scanning and Transmission Electron Microscopy

Scanning electron microscopy (SEM) and transmission electron microscopy (TEM) were used to investigate the crystallinity of the γ-Sn_3N_4 samples. All products prepared using Mg_3N_2 exhibit a better crystallinity than those synthesized with Li_3N or Ca_3N_2 (Figure 4). Crystallites of up to 7 μm in diameter were obtained via the Mg_3N_2 route.

SEM images show that the crystallinity of the products of the reactions with Mg_3N_2 improves with decreasing reaction temperature and when a tin flux is used (Figure 4). As the reaction temperature increases, only a few isolated crystallites of larger size are present, while the size of the majority of crystallites decreases. The significant improvement of the crystallinity due to the tin flux supports the assumption that the solubility behavior of the Mg-Sn–N system has a considerable influence on the synthesis, in particular on the yield. Furthermore, using a higher argon flow rate and thus a shorter reaction time seems to improve the crystallinity (Figure S12). While SEM is not suitable to distinguish the crystallite sizes of the products synthesized via the Li_3N route, TEM images (Figure S13) reveal a similar trend but with overall much smaller crystallites.

All observations are in accordance with the noted reflection broadening in the PXRD patterns.

Single-Crystal X-ray Diffraction

Because of the good crystallinity of the samples synthesized at lower temperatures with Mg_3N_2, these crystals were clearly visible and could be isolated with the help of an optical microscope. Subsequently, it was possible to measure single-crystal diffraction data. Previously, only powder diffraction and neutron diffraction data of γ-Sn_3N_4 were available. In accordance with the structure model determined by Scotti *et al.*, the structure was solved and refined in cubic space group $Fd\bar{3}m$ (no. 227) with a lattice parameter of 9.0221(5) Å.[36,53]

The tin atoms occupy two crystallographically independent sites (8*b* and 16*c*) with fixed coordinates. The nitrogen atoms occupy the Wyckoff position 32*e* with $x=y=z$ with $x(N)=0.2406(4)$. The $x(N)$ value is in agreement with that reported by Scotti et al. ($x(N)=0.24050(6)$, Table S8).[36] The crystallographic data are given in Table 2. Wyckoff positions, atomic coordinates, anisotropic displacement parameters, interatomic distances and angles are given in Tables S5–S7

Elemental Analysis

Elemental analysis was performed using energy-dispersive X-ray (EDX) spectroscopy, dynamic flash combustion analysis, and the hot gas extraction method. Results of the measurements are given in Tables S9, S10, S11 and Figure S14.

For all γ-Sn_3N_4 samples prepared via the Mg_3N_2 route, an average tin content of 43(1) at-% was detected by EDX measurements, which is consistent with the expected value. The average nitrogen contents are between 53(2) and 55(1) at-% and thus slightly lower than the expected value of 57 at-%. Nevertheless, considering the measurement accuracy

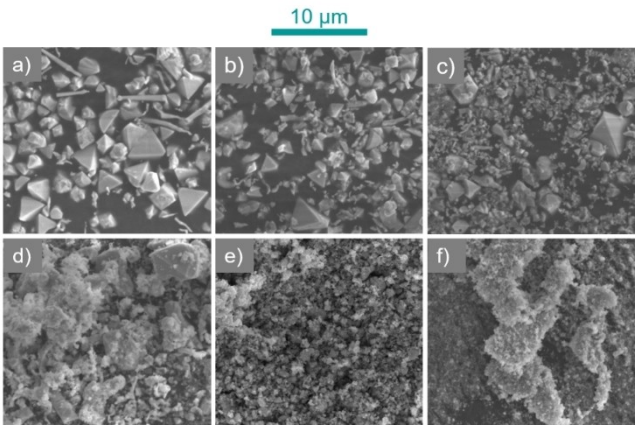

Figure 4. SEM images of γ-Sn_3N_4 prepared by reaction of $SnCl_4$ and Mg_3N_2 in a tin flux at a) 275 °C, b) 325 °C and c) 375 °C, as well as SEM images of γ-Sn_3N_4 prepared at 325 °C d) by reaction of $SnCl_4$ and Mg_3N_2 without using a tin flux and by reaction of $SnCl_4$ with e) Li_3N and f) Ca_3N_2 in a tin flux.

Table 2. Crystallographic data from single-crystal refinement of γ-Sn_3N_4 (standard deviations in parentheses).

Sum formula	γ-Sn_3N_4
crystal system	cubic
molecular weight/g mol^{-1}	412.11
space group	$Fd\bar{3}m$ (no. 227)
lattice parameter a/Å	9.0221(5)
cell volume/Å^3	734.38(12)
formula units per cell	8
calculated density/g cm^{-3}	7.45
μ/mm^{-1}	20.1
T_{min}/T_{max}	0.532/0.747
radiation	Mo-Kα ($\lambda=0.71073$)
temperature/K	293(2)
F(000)	1424
θ range/°	$7.823 \leq \theta \leq 77.22$
total no. of reflections	2807
independent reflections ($>2\sigma$)	64(57)
refined parameters	7
R_{int}; R_σ	0.0441; 0.0102
$R1$ (all data); $R1$ ($F^2>2\sigma(F^2)$)	0.0163; 0.0116
$wR2$ (all data); $wR2$ ($F^2>2\sigma(F^2)$)	0.0245; 0.0237
Goodness of fit	1.290
$\Delta\rho_{max}$; $\Delta\rho_{min}$/e Å^{-3}	0.55; −0.66

of this method, especially for light elements, the experimental values are in good agreement with the theoretical value. Furthermore, it should be noted that at some measurement points it was observed that crystallites decomposed in the electron beam. Consequently, a slightly diminished nitrogen content may also be the result of incipient decomposition during the measurement. In addition to tin and nitrogen, small amounts of oxygen and, at a few measuring points, chlorine (< 0.5 at-%) were detected. Both, the oxygen and chlorine contents are most likely caused by the washing treatment with concentrated HCl and H_2O. The washing treatment can induce surface hydrolysis, leading to partial substitution of nitrogen by oxygen at the surface. It is also possible that the somewhat too low nitrogen content is due to surface hydrolysis.

Furthermore, an EDX measurement was carried out on a sample synthesized at 325 °C from Li_3N and $SnCl_4$ in order to investigate potential differences between the products of different routes. The average tin content (42(1) at-%) is, within uncertainty, in agreement with the theoretical value. However, the nitrogen content is much lower than expected (46(2) at-%) and a high oxygen content (12(3) at-%) was detected. Due to the significantly smaller crystallites in the samples prepared via the Li_3N route, the surface has an enhanced influence on the measurements. Therefore, the elevated oxygen content and the resulting lower nitrogen content may possibly be attributed to surface hydrolysis. Moreover, it can be assumed that the self-adhesive carbon pad also exerts an influence on the oxygen content because of the small crystallites. Nevertheless, substitution of nitrogen by oxygen may also be a contributing factor to the elevated oxygen content. It should be noted, that EDX values are most reliable for large crystals with polished surfaces. Consequently, the measurement accuracy decreases with decreasing crystallinity.

Due to the limited accuracy of EDX spectroscopy for light elements and poorly crystalline samples, dynamic flash combustion and hot gas extraction analyses were performed to determine the nitrogen, oxygen and hydrogen content of different γ-Sn_3N_4 samples. The results are shown in Tables S10 and S11 and Figure S14.

For samples prepared using Mg_3N_2 as precursor, nitrogen contents between 53(1) and 57(2) at-% were obtained. Additionally, oxygen contents between 2(1) and 4(1) at-% and hydrogen contents between 2(1) and 8(1) at-% were obtained. The nitrogen contents are in good agreement with the expected value of 57 at-% for pure stoichiometric γ-Sn_3N_4 and surpass all previously reported values for bulk γ-Sn_3N_4, highlighting the quality of the products.[13,54] Consistent with the measured oxygen and hydrogen contents, the slightly lower-than-expected nitrogen contents are likely due to surface hydrolysis and sorption of humidity to the surface.

Analyses of the samples synthesized via the Li_3N route resulted in nitrogen contents between 48(2) and 52(1) at-%, oxygen contents between 6(1) and 10(1) at-% and hydrogen contents between 4(1) and 8(1) at-%. The nitrogen contents are lower, while the oxygen contents higher than for the products synthesized via the Mg_2N_3 route. This is in agreement with the EDX measurements. As discussed above, the measured values could be caused by surface hydrolysis and the sorption of humidity to the surface, as the crystallinity of the products synthesized via the Li_3N route is poorer, resulting in a larger surface area. This hypothesis is supported by the fact that the hydrogen contents are also higher than those of the products synthesized via the Mg_3N_2 route.

In order to gain further insight into the origin of the reflection shift and splitting observed in the powder diffraction data, several samples prepared at different temperatures were measured. However, no discernible trend was observed in either nitrogen or oxygen content with respect to the reaction temperature.

X-ray Photoelectron Spectroscopy

X-ray photoelectron spectroscopy (XPS) measurements were conducted to examine the bonding environment of tin and to gain further insights into whether the too low nitrogen content and the presence of oxygen are due to surface hydrolysis (Figure S15). Nitrogen deficiencies in γ-Sn_3N_4 would lower the oxidation state of Sn in their vicinity.

For measurements, samples synthesized at 325 °C from the reactions of $SnCl_4$ with Mg_3N_2 and Li_3N, respectively, were used. The results are discussed based on the data of the product synthesized via the Mg_3N_2 route, since both spectra show similar peaks.

The Sn 3d and N 1s spectra are given in Figure 5. The binding energy of the main component of the Sn $3d_{5/2}$ peak ($E_B = 486.8$ eV) is in accordance with values reported for γ-Sn_3N_4.[37,43,45,55,56] However, the binding energies of Sn(II) and Sn(IV) exhibit only slight differences, therefore the presence of Sn(II) cannot be excluded based on the obtained data.[56–58] The small shoulder at lower binding energy ($E_B = 484.6$ eV) can be assigned to Sn metal, which most likely originates from decomposition of γ-Sn_3N_4 in ultra-high vacuum, potentially influenced by heat generated by the X-ray cathode filament or the X-ray radiation itself.[55] The N 1s peak suggests that most of the detected nitrogen is bonded to tin ($E_B = 397.3$ eV).[37,43,45,55,56] The other components at higher binding energy can be assigned to nitrogen associated with carbon, which is due to surface contamination, probably caused by washing the samples with ethanol.[56]

In addition to the Sn 3d and N 1s peaks, a broad O 1s signal with a maximum around 531.5 eV was detected. It can be assigned to various contributions of water and hydroxyl species, resulting from water adsorption on the surface.[37,57,59,60] Peaks of oxygen bonded to Sn^{4+} or Sn^{2+} are expected to occur at lower binding energies (~530 eV).[37,57,58]

The relative composition of the detected volume was quantified as 45 at-% Sn, 34 at-% N and 21 at-% O. Given an estimated detection depth of approximately 2.5 lattice parameters, the low oxygen contents detected by EDX and hot gas extraction analysis must predominantly be located at the outermost surface. These results support the assumption that the slightly deficient nitrogen contents are due to surface hydrolysis processes.

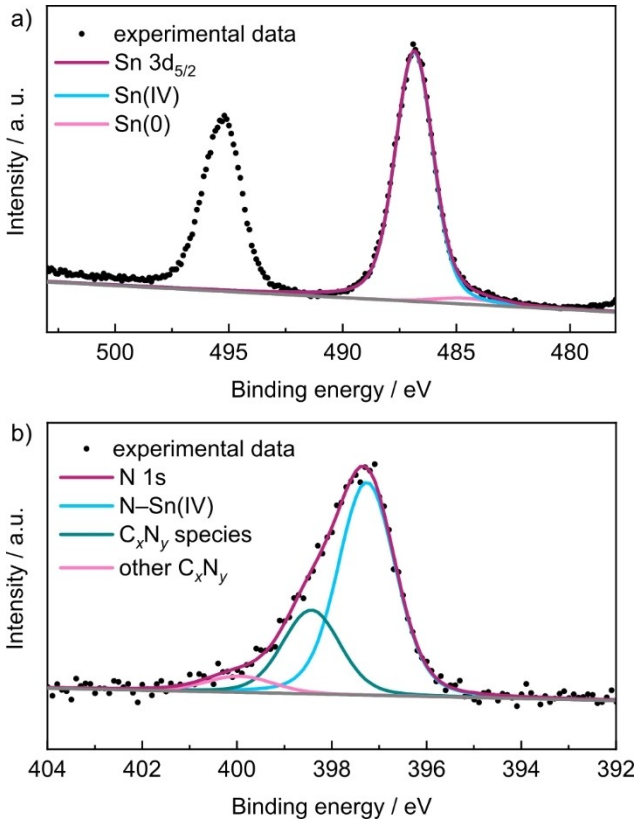

Figure 5. X-ray photoelectron spectra with corresponding fits from the (a) Sn 3d and (b) N 1s regions of γ-Sn_3N_4 prepared at 325 °C using Mg_3N_2 as the nitrogen source.

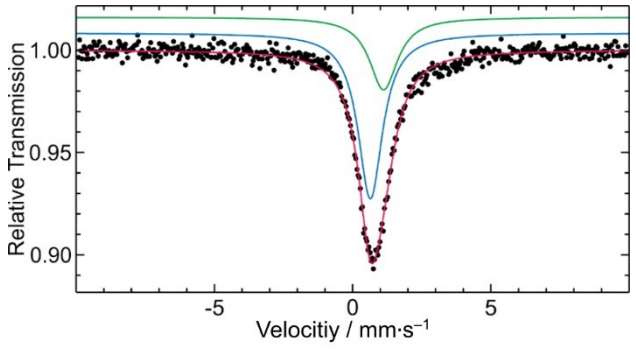

Figure 6. Experimental (black dots) and simulated (colored lines) ^{119}Sn Mössbauer spectrum of γ-Sn_3N_4 prepared at 325 °C via the Mg_3N_2 route.

Table 3. Fitting parameters of a ^{119}Sn Mössbauer spectroscopic measurement at 78 K for the γ-Sn_3N_4 sample prepared at 325 °C using Mg_3N_2 as nitrogen-containing precursor. δ = isomer shift, ΔE_Q = electric quadrupole splitting, Γ = experimental line width. Parameters marked with an asterisk were kept fixed during the fitting procedure.

Signal	δ/mm s^{-1}	ΔE_Q/mm s^{-1}	Γ/mm s^{-1}
Sn1 (green)	1.12(1)	0*	1.24(5)
Sn2 (blue)	0.64(1)	0*	1.08(2)

For the sample prepared via the Li_3N route, the relative composition of the detected volume was quantified as 45 at-% Sn, 27 at-% N and 28 at-% O. The higher oxygen content, compared to the sample prepared via the Mg_3N_2 route, aligns with the smaller crystallite sizes typically obtained via the Li_3N route. However, the greater nitrogen deficit and higher oxygen contents observed for these samples through elemental analyses, compared to those prepared via Mg_3N_2 route, suggest that O_N substitution cannot be entirely ruled out, especially given the surface sensitivity of XPS.

Mössbauer Spectroscopy

As XPS is a surface sensitive method and that the binding energies of Sn(II) and Sn(IV) differ only slightly, ^{119}Sn Mössbauer spectroscopic measurements were performed to experimentally verify the Sn oxidation state of +IV on bulk samples. The ^{119}Sn spectrum (78 K data) of a γ-Sn_3N_4 sample prepared via the Mg_3N_2 route at 325 °C is presented in Figure 6. The corresponding fitting parameters are summarized in Table 3.

The spectrum shows one broader signal in the isomer shift region of tetravalent tin compounds. This is consistent with the splitting $Sn_3N_4 \equiv 3\ Sn^{4+} + 4\ N^{3-}$. But, the line width is too large to be assigned to a single Sn(IV) site. The tin atoms occupy two crystallographically independent sites in the spinel type structure, i.e., $Sn1^{4+}$ on 8*b* (site symmetry $\bar{4}3\,m$) and $Sn2^{4+}$ on 16*c* (site symmetry.$\bar{3}m$) in 1:2 ratio. Thus, two independent Sn(IV) signals were introduced and their area was fixed in a 1:2 ratio during fitting (without quadrupole splitting due to the cubic site symmetry). The larger signal corresponds to the octahedral $Sn2@N_6$ site and the smaller one to tetrahedral $Sn1@N_4$. The higher degree of nitride coordination for Sn2 decreases the *s* electron density at the Sn2 nuclei, in agreement with the lower isomer shift (0.64(1) mm s^{-1} for Sn2 vs. 1.12(2) mm s^{-1} for Sn1). This is essentially similar to the course of the isomer shifts observed for $Sn@S_4$ and $Sn@S_6$ coordination in various tin-based sulphides.[61]

Our measured isomer shift values are similar to those observed for tin nitride films prepared as electrode materials for lithiation.[11,62] A ^{119}Sn Mössbauer spectrum was already reported in the dissertation of Scotti; however, the spectrum was fitted with a single signal at $\delta = 0.6$ mm s^{-1} without resolving the crystallographically independent tin sites.[54] In contrast to cassiterite (SnO_2) we observe a clear increase of the isomer shifts for the two tin sites, a consequence of the lower electronegativity of nitrogen (3.04 on the Pauling scale) as compared to oxygen (3.44).[63]

In addition, we measured ^{119}Sn spectra (78 K data) of γ-Sn_3N_4 samples which were synthesized via the Li_3N route at T = 275, 325, 350 and 400 °C. The spectra are presented in Figure S16. The corresponding fitting parameters are summarized in Table S12.

The overall shape of the spectra is similar and they were reproduced with the same model. Similar to the spectrum of the sample prepared via the Mg_3N_2 route, the Sn(IV) signals were reproduced with two spectral components accounting for

$Sn1^{4+}$ on 8*b* and $Sn2^{4+}$ on 16*c*. The isomer shift values of all five investigated samples are in good agreement. The signal areas were refined without constraints and they reproduce the Sn1:Sn2 ratio of 1:2.

In contrast to the sample prepared via the Mg_3N_2 route, the four samples prepared via the Li_3N route show an additional spectral component (13–14%) in the higher isomer shift region. These sub-signals at $\delta = 2.71$ mm s^{-1} are subjected to quadrupole splitting of $\Delta E_Q = 1.45$ mm s^{-1}. These spectral parameters are typical for a Sn(II) species with lone-pair character. A comparison with literature values shows reasonable agreement with those of SnO.[61,64,65]

X-ray Emission and Absorption Spectroscopy

X-ray emission (XES) and absorption (XAS) spectroscopy measurements and calculations were carried out to examine samples synthesized via the Li_3N route for possible SnO contamination and to determine if there is any noticeable substitution of nitrogen by oxygen. Several samples synthesized at different temperatures were analyzed. The results are shown in Figures 7, S17 and S18. To address the known underestimation of band gaps in spectra calculated from the PBE-GGA functional, the calculated spectra were shifted to align with the features and peak positions of the measured spectra. The measured N Kα XES and N K-edge XAS spectra and the calculated spectra of defect-free γ-Sn_3N_4 are in excellent agreement (Figure 7a). Crystal parameters listed in Table S5 were used for the DFT calculations. The calculated N K-edge XAS spectrum in the presence of an N 1s core hole (solid line) closely matches the measured XAS spectra. This is expected since the final state of the absorption process has a core hole present, perturbing the crystal and shifting the spectral weight to slightly lower energies.

There are no observable differences between the samples synthesized at different temperatures. The agreement between the calculated and empirical data suggests minimal oxygen contamination and confirms that the products are free of other nitrogen-containing materials.

The valence and conduction band edges were identified using the second derivative method to determine the band gap.[66,67] An experimental band gap of 1.5 ± 0.2 eV was obtained. This agrees with a previously reported result for γ-Sn_3N_4 using the same method.[15] The calculated band gap using the PBE-GGA approach is 0.56 eV, which is known to underestimate the band gap. In contrast, the calculation using the mBJ exchange-correlation functional yields a value of 1.60 eV, which is in good agreement with the experimental result.

Further DFT calculations were performed to investigate how the presence of Sn vacancies and O impurities affect the XAS spectral profile. Figure 7b shows the measured N K-edge XAS spectrum and the calculated spectra of five different models. These models include (i) a defect-free γ-Sn_3N_4, (ii) a model with one Sn vacancy (at octahedral site) and O for N substitution to preserve local charge neutrality [γ-$Sn_{3-x}(N_{1-x}O_x)_4$ with $x = 4/32$], and (iii) another version without Sn vacancy that does not have

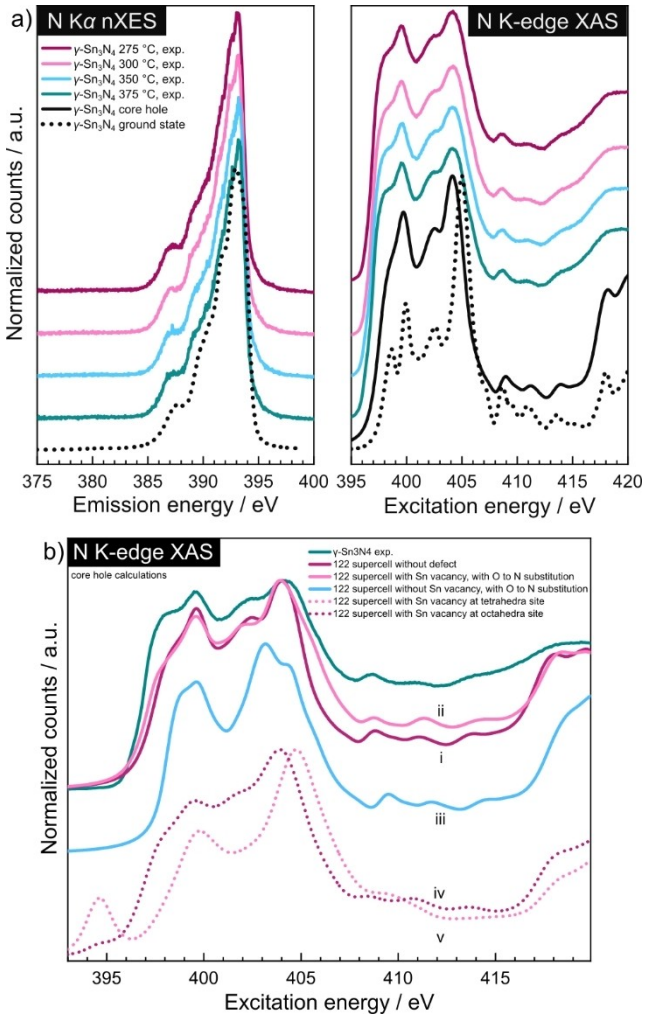

Figure 7. a) Empirical non-resonant N Kα XES spectra of γ-Sn_3N_4, synthesized at different temperatures (excitation energy of 440 eV) (colored lines) and calculated XES spectrum of γ-Sn_3N_4 (black dots) (left). On the right, the measured N K-edge XAS spectra of γ-Sn_3N_4, synthesized at different temperatures (colored lines) and the calculated XAS spectrum of γ-Sn_3N_4 for the ground state and core hole (black line and dots) are shown. b) Calculated N K-edge XAS spectra of γ-Sn_3N_4 with Sn vacancies and O impurities.

local charge neutrality [γ-$Sn_3(N_{1-x}O_x)_4$ with $x = 4/32$]. In addition, in (iv) and (v) two calculations for Sn vacancies at each non-equivalent Sn site but without any O impurity are shown as dotted lines. In this case the missing charge was added to the background.

The calculated N K-edge XAS spectra of (i) defect-free γ-Sn_3N_4 and (ii) charge-neutral γ-$Sn_{3-x}(N_{1-x}O_x)_4$ differ only slightly from one another and are both in excellent agreement with the measured spectrum (Figure 7b). Since the XAS spectra of models (i) and (ii) are experimentally indistinguishable, we cannot draw definitive conclusions about the presence or absence of oxygen for nitrogen substitution in the spinel structure of γ-Sn_3N_4. The subsequent model (iii), depicted in light blue, features only O_N substitutions, without the presence of a Sn vacancy. The agreement between the calculated and experimental spectrum is not as good as for the previous two models (i and ii). Models (iv) and (v) (dotted lines) only assume

a Sn vacancy, which is calculated for a tetrahedral and octahedral Sn site, respectively. The spectrum resulting from model (iv) captures the general features of the measured N K-edge XAS data but not the height of dominant peaks. A Sn vacancy on the tetrahedral site appears to lead to a stronger distortion. The spectrum exhibits poor alignment with the experimental data. An additional peak at ~394.5 eV is observed and the most intense peak is shifted to a higher energy. In conclusion models iii–v are unlikely to be realized.

Moreover, DFT calculations were carried out to examine the effect of different amounts of oxygen impurities in the vicinity of a Sn(IV) vacancy (at octahedral site) and ascertain whether the position of the O_N substitution affects the spectrum. The results are shown in Figure S17 (models vi–viii). The level of agreement between the calculated spectra and the measured spectrum decreases with increasing nitrogen substitution by oxygen. Furthermore, the results demonstrate that the position of the O_N substitution has a considerable impact on the N K-edge spectrum. In both models (ii) and (vii), four N atoms surrounding the Sn vacancy were replaced with O atoms. Only the position of the substituted N was altered.

To gain further insight into the oxygen contamination, O K-edge measurements were performed on tin nitride samples synthesized at different temperatures via the Li_3N route and on SnO and SnO_2 reference samples (Figure S18). Furthermore, DFT calculations were performed for $Sn_3(N_{1-x}O_x)_4$ with oxygen levels ranging from 1% to 3%, as well as for the charge-neutral γ-$Sn_{3-x}(N_{1-x}O_x)_4$ model. All O K-edge spectra of the tin nitride samples are sharing a similar spectral shape. The XES spectra are in good agreement with the spectra of the SnO and SnO_2 samples. The XAS spectra, on the contrary, show considerable differences, especially with respect to the spectrum of SnO_2. It is therefore assumed that SnO_2 is not (or only in very small quantities) present as an impurity. Small amounts of SnO could be present, but not as the only source of oxygen. A better agreement with the experimental XAS spectra can be seen when they are compared with the calculated spectra for $Sn_3N_{4-x}O_x$ with $1\% \leq x \leq 3\%$ as well as for the charge-neutral γ-$Sn_{3-x}(N_{1-x}O_x)_4$ model (ii). However, the calculated O Kα XES spectra of γ-$Sn_3(N_{1-x}O_x)_4$ with $1\% \leq x \leq 3\%$ do not match well with the experiment. In contrast, the calculated spectrum of the charge-neutral γ-$Sn_{3-x}(N_{1-x}O_x)_4$ model (ii) is in good agreement with the measured spectrum. These results suggest that some oxygen may have been incorporated into the tin nitride synthesized via the Li_3N route. As previously mentioned, the reactor is likely to be the main source of this oxygen contamination, due to the interaction of lithium with the glass. Future studies targeting the synthesis of ternary tin oxynitrides may allow for tuning of properties. By synthesizing γ-Sn_3N_4 via the Mg_3N_2 route, contamination by oxygen caused by the reactor is avoided.

The results of the calculations indicate that both Sn vacancies and O impurities have an influence on the N K-edge XAS spectrum, although the O impurities appear to exert a more pronounced effect. Both the amount of O_N substitution as well as the specific position at which O would substitute N have a measurable influence on the N K-edge spectra.

Conclusions

Using γ-Sn_3N_4 as a model compound, a promising new approach for the synthesis of nitrides is reported. The presented synthesis method is simple, easily scalable, yields phase-pure bulk material and is suitable for thermally less stable nitrides. Moderate temperatures during the reaction are achieved by slow mixing of reactive starting materials. This is done by diluting a volatile starting material with an inert carrier gas. In addition, the heat generated during the reaction is removed by the carrier gas flow. The reaction and crystallization can be further enhanced by the use of a flux. In contrast to solvothermal reactions, impurities caused by solvents are avoided.

γ-Sn_3N_4 was synthesized by metathesis of argon-diluted $SnCl_4$ and various binary nitrides (Li_3N, Ca_3N_2 and Mg_3N_2). Mg_3N_2 was found to be the best starting material for the synthesis of phase-pure, crystalline γ-Sn_3N_4. Yields of up to 82% were obtained. Due to the good crystallinity, we were able to collect single-crystal X-ray diffraction data of γ-Sn_3N_4, which were previously not available. EDX spectroscopy, dynamic flash combustion analysis and hot gas extraction analysis were carried out for elemental analysis. The Sn oxidation state of +IV was verified by Mössbauer spectroscopy.

The experimental set-up is highly adaptable, allowing convenient modifications. The only requirement is that one of the starting materials, liquid or solid, has a high enough vapor pressure to be evaporated in a glass apparatus. The synthesis method could also provide access to new ternary nitrides. In addition, further scaling experiments could be carried out by increasing the batch size and, if necessary, using a larger reactor. This approach is likely to yield significantly larger quantities of product. Thus, the method presented in this article offers a wide range of possibilities for the synthesis of nitrides.

Supporting Information Summary

The authors have cited additional references within the Supporting Information.[68–102]

Acknowledgements

We gratefully acknowledge Amalina T. Buda and Christian Minke for EDX measurements (both at Department of Chemistry, LMU Munich) and Klaudia Opri, Tillmann Rathfelder and Prof. Dr. Rainer Niewa for quantitative analysis of γ-Sn_3N_4 via the hot gas extraction method (all at Institute for Inorganic Chemistry, University of Stuttgart). Furthermore, we thank Dr. Monika M. Pointner for TEM measurements and Felix Drötboom for experimental assistance (both at Department of Chemistry, LMU Munich). The authors acknowledge funding support from the Deutsche Forschungsgemeinschaft (DFG, German Research Foundation) under Germany's Excellence Strategy-EXC 2089/1-390776260 (e-Conversion). We thank the Natural Sciences and Engineering Research Council of Canada (NSERC) and the

Canada Research Chair program for financial support the Graham HPC cluster and the Digital Research Alliance of Canada for providing computing resources. The Canadian Light Source is supported by the Canada Foundation for Innovation (CFI), NSERC, the National Research Council (NRC), the Canadian Institutes of Health Research (CIHR), the Government of Saskatchewan, and the University of Saskatchewan. Open Access funding enabled and organized by Projekt DEAL.

Conflict of Interests

The authors declare no conflict of interest.

Data Availability Statement

The data that support the findings of this study are available in the supplementary material of this article.

Keywords: Metathesis · Moessbauer spectroscopy · Synthesis design · Tin(IV) nitride · X-ray absorption and emission spectroscopy

[1] A. L. Greenaway, C. L. Melamed, M. B. Tellekamp, R. Woods-Robinson, E. S. Toberer, J. R. Neilson, A. C. Tamboli, *Annu. Rev. Mater. Res.* **2021**, *51*, 591–618.
[2] S. Nakamura, T. Mukai, M. Senoh, *Appl. Phys. Lett.* **1994**, *64*, 1687–1689.
[3] K. Komeya, M. Matsui, in *Materials Science and Technology* (Eds.: R. W. Cahn, P. Haasen, E. J. Kramer), Wiley-VCH, Weinheim, **1994**, pp. 518–565.
[4] R. N. Katz, *Science* **1980**, *208*, 841–847.
[5] Y. Hinuma, T. Hatakeyama, Y. Kumagai, L. A. Burton, H. Sato, Y. Muraba, S. Iimura, H. Hiramatsu, I. Tanaka, H. Hosono, F. Oba, *Nat. Commun.* **2016**, *7*, 11962.
[6] A. Zakutayev, *J. Mater. Chem. A* **2016**, *4*, 6742–6754.
[7] W. Sun, C. J. Bartel, E. Arca, S. R. Bauers, B. Matthews, B. Orvananos, B. R. Chen, M. F. Toney, L. T. Schelhas, W. Tumas, J. Tate, A. Zakutayev, S. Lany, A. M. Holder, G. Ceder, *Nat. Mater.* **2019**, *18*, 732–739.
[8] C. Zhixing, Q. Weiliang, C. H. Pang, T. Thomas, T. Wu, S. Liu, M. Yang, *Adv. Funct. Mater.* **2021**, *31*, 2100553.
[9] Y. Wu, P. Lazić, G. Hautier, K. A. Persson, G. Ceder, *Energy Environ. Sci.* **2013**, *6*, 157–168.
[10] A. L. Greenaway, S. Ke, T. Culman, K. R. Talley, J. S. Mangum, K. N. Heinselman, R. S. Kingsbury, R. W. Smaha, M. K. Gish, E. M. Miller, K. A. Persson, K. A. Persson, J. M. Gregoire, S. R. Bauers, J. B. Neaton, A. C. Tamboli, A. Zakutayev, *J. Am. Chem. Soc.* **2022**, *144*, 13673–13687.
[11] L. Baggetto, N. A. M. Verhaegh, R. A. H. Niessen, F. Roozeboom, J.-C. Jumas, P. H. L. Notten, *J. Electrochem. Soc.* **2010**, *157*, A340–A347.
[12] X. Li, A. L. Hector, J. R. Owen, S. I. U. Shah, *J. Mater. Chem. A* **2016**, *4*, 5081–5087.
[13] S. D. S. Fitch, G. Cibin, S. P. Hepplestone, N. Garcia-Araez, A. L. Hector, *J. Mater. Chem. A* **2020**, *8*, 16437–16450.
[14] Y. Zhu, X. He, Y. Mo, *Adv. Sci.* **2017**, *4*, 1600517.
[15] T. D. Boyko, A. Hunt, A. Zerr, A. Moewes, *Phys. Rev. Lett.* **2013**, *111*, 097402.
[16] N. C. George, K. A. Denault, R. Seshadri, *Annu. Rev. Mater. Res.* **2013**, *43*, 481–501.
[17] F. Liu, X. Zhao, P. Shi, L. Li, Q. Dong, M. Tian, Y. Wu, X. Sun, *Batteries* **2023**, *9*, 396.
[18] A. Zakutayev, S. R. Bauers, S. Lany, *Chem. Mater.* **2022**, *34*, 1418–1438.
[19] T. Andersen, H. K. Haugen, H. Hotop, *J. Phys. Chem. Ref. Data* **1999**, *28*, 1511–1533.
[20] H. Hotop, W. C. Lineberger, *J. Phys. Chem. Ref. Data* **1985**, *14*, 731–750.
[21] S. H. Elder, F. J. DiSalvo, L. Topor, A. Navrotsky, *Chem. Mater.* **1993**, *5*, 1545–1553.
[22] L. E. Toth, *Transition Metal Carbides and Nitrides*, Academic Press, New York, **1971**.
[23] W. Sun, S. T. Dacek, S. P. Ong, G. Hautier, A. Jain, W. D. Richards, A. C. Gamst, K. A. Persson, G. Ceder, *Sci. Adv.* **2016**, *2*, e1600225.
[24] W. Sun, A. Holder, B. Orvañanos, E. Arca, A. Zakutayev, S. Lany, G. Ceder, *Chem. Mater.* **2017**, *29*, 6936–6946.
[25] C. L. Dezelah Iv, O. M. El-Kadri, M. J. Heeg, C. H. Winter, *J. Mater. Chem.* **2004**, *14*, 3167–3176.
[26] J. Choi, E. G. Gillan, *Inorg. Chem.* **2005**, *44*, 7385–7393.
[27] J. Choi, E. G. Gillan, *Inorg. Chem.* **2009**, *48*, 4470–4477.
[28] E. G. Gillan, R. B. Kaner, *Inorg. Chem.* **1994**, *33*, 5693–5700.
[29] A. L. Hector, I. P. Parkin, *Polyhedron* **1995**, *14*, 913–917.
[30] E. G. Gillan, R. B. Kaner, *Chem. Mater.* **1996**, *8*, 333–343.
[31] J. Hu, Q. Lu, K. Tang, S. Yu, Y. Qian, G. Zhou, X. Liu, *J. Amer. Ceram. Soc.* **2000**, *83*, 430–432.
[32] Y. Xie, Y. Qian, W. Wang, S. Zhang, Y. Zhang, *Science* **1996**, *272*, 1926–1927.
[33] F. Kawamura, M. Imura, H. Murata, N. Yamada, T. Taniguchi, *Eur. J. Inorg. Chem.* **2019**, *2020*, 446–451.
[34] B. Mazumder, P. Chirico, A. L. Hector, *Inorg. Chem.* **2008**, *47*, 9684–9690.
[35] B. Mazumder, A. L. Hector, *J. Mater. Chem.* **2008**, *18*, 1392–1398.
[36] N. Scotti, W. Kockelmann, J. Senker, S. Trassel, H. Jacobs, *Z. Anorg. Allg. Chem.* **1999**, *657*, 1435–1439.
[37] F. Qu, Y. Yuan, M. Yang, *Chem. Mater.* **2017**, *29*, 969–974.
[38] C. M. Caskey, J. A. Seabold, V. Stevanović, M. Ma, W. A. Smith, D. S. Ginley, N. R. Neale, R. M. Richards, S. Lany, A. Zakutayev, *J. Mater. Chem. C* **2015**, *3*, 1389–1396.
[39] A. Zerr, G. Miehe, *Phil. Trans. R. Soc. A* **2023**, *381*, 20220330.
[40] S. B. Nam, D. C. Reynolds, C. W. Litton, R. J. Almassy, T. C. Collins, C. M. Wolfe, *Phys. Rev. B* **1976**, *13*, 761–767.
[41] R. Juza, H. Hahn, *Z. Anorg. Allg. Chem.* **1940**, *244*, 133–148.
[42] R. Kamei, T. Migita, T. Tanaka, K. Kawabata, *Vacuum* **2000**, *59*, 764–770.
[43] Y. Inoue, M. Nomiya, O. Takai, *Vacuum* **1998**, *51*, 673–676.
[44] T. Maruyama, T. Morishita, *Appl. Phys. Lett.* **1996**, *69*, 890–891.
[45] T. Maruyama, T. Morishita, *J. Appl. Phys.* **1995**, *77*, 6641–6645.
[46] L. Maya, *J. Vac. Sci. Technol. A* **1993**, *11*, 604–608.
[47] R. S. Lima, P. H. Dionisio, W. H. Schreiner, C. Achete, *Solid State Commun.* **1991**, *79*, 395–398.
[48] R. G. Gordon, D. M. Hoffman, U. Riaz, *Chem. Mater.* **1992**, *4*, 68–71.
[49] N. Takahashi, K. Terada, T. Nakamura, *J. Mater. Chem.* **2000**, *10*, 2835–2837.
[50] M. P. Shemkunas, G. H. Wolf, K. Leinenweber, W. T. Petuskey, *J. Amer. Ceram. Soc.* **2002**, *85*, 101–104.
[51] M. G. Kanatzidis, R. Pöttgen, W. Jeitschko, *Angew. Chem. Int. Ed.* **2005**, *44*, 6996–7023; *Angew. Chem.* **2005**, *6117*, 7156–7184.
[52] E. G. Rognerud, C. L. Rom, P. K. Todd, N. R. Singstock, C. J. Bartel, A. M. Holder, J. R. Neilson, *Chem. Mater.* **2019**, *31*, 7248–7254.
[53] Deposition Number 2403131 contain the supplementary crystallographic data for this paper. These data are provided free of charge by the joint Cambridge Crystallographic Data Centre and Fachinformationszentrum Karlsruhe Access Structures service.
[54] N. Scotti, PhD Thesis, University of Dortmund (DE) **1999**.
[55] D. Lützenkirchen-Hecht, R. Frahm, *Thin Solid Films* **2005**, *493*, 67–76.
[56] C. M. Caskey, A. Holder, S. Shulda, S. T. Christensen, D. Diercks, C. P. Schwartz, D. Biagioni, D. Nordlund, A. Kukliansky, A. Natan, D. Prendergast, B. Orvananos, W. Sun, X. Zhang, G. Ceder, D. S. Ginley, W. Tumas, J. D. Perkins, V. Stevanovic, S. Pylypenko, S. Lany, R. M. Richards, A. Zakutayev, *J. Chem. Phys.* **2016**, *144*, 144201.
[57] Q.-H. Wu, J. Song, J. Kang, Q.-F. Dong, S.-T. Wu, S.-G. Sun, *Mater. Lett.* **2007**, *61*, 3679–3684.
[58] J. Szuber, G. Czempik, R. Larciprete, D. Koziej, B. Adamowicz, *Thin Solid Films* **2001**, *391*, 198–203.
[59] W. J. Kim, W. H. Koo, S. J. Jo, C. S. Kim, H. K. Baik, J. Lee, S. Im, *Appl. Surf. Sci.* **2005**, *252*, 1332–1338.
[60] M. Kwoka, L. Ottaviano, M. Passacantando, S. Santucci, G. Czempik, J. Szuber, *Thin Solid Films* **2005**, *490*, 36–42.
[61] P. E. Lippens, *Phys. Rev. B* **1999**, *60*, 4576–4586.
[62] L. Baggetto, J.-C. Jumas, H. T. Hintzen, P. H. L. Notten, *Electrochim. Acta* **2010**, *55*, 6617–6631.
[63] J. Emsley, *The Elements*, Oxford University Press, Oxford, **1999**, p. 142.
[64] C. G. Davies, J. D. J. Donaldson, *Chem. Soc. (A)* **1968**, 946–948.
[65] N. N. Greenwood, T. C. Gibb, *Mössbauer Spectroscopy*, Chapman and Hall, London, **1971**, p. 388.

[66] T. D. Boyko, E. Bailey, A. Moewes, P. F. McMillan, *Phys. Rev. B* **2010**, *81*, 155207.
[67] E. Z. Kurmaev, R. G. Wilks, A. Moewes, L. D. Finkelstein, S. N. Shamin, J. Kuneš, *Phys. Rev. B* **2008**, *77*, 165127.
[68] H. M. Rietveld, *J. Appl. Crystallogr.* **1969**, *2*, 65–71.
[69] A. A. Coelho, *TOPAS-Academics*, Version 6, Brisbane, Australien, **2016**.
[70] R. W. Cheary, A. A. Coelho, *J. Appl. Crystallogr.* **1992**, *25*, 109–121.
[71] R. W. Cheary, A. A. Coelho, J. P. Cline, *J. Res. Natl. Inst. Stand. Technol.* **2004**, *109*, 1–25.
[72] SAINT, Data Integration Software, Madison, Wisconsin, USA, **1997**.
[73] Bruker-AXS, *APEX3*, Vers. 2018.2011–2010, Madison, WI, USA, **2018**.
[74] G. M. Sheldrick, *SADABS*: Multi-Scan Absorption Correction, Vers. 2016/2012, Bruker-AXS, Madison, WI, USA, **2016**.
[75] L. Krause, R. Herbst-Irmer, G. M. Sheldrick, D. Stalke, *J. Appl. Cryst.* **2015**, *48*, 3–10.
[76] Bruker-AXS, *XPREP*: Reciprocal Space Exploration, Vers. 2014/2012, Madison, WI, USA, **2014**.
[77] G. M. Sheldrick, *Acta Crystallogr., Sect. A: Fond. Adv.* **2015**, *71*, 3–8.
[78] G. M. Sheldrick, *Acta Crystallogr., Sect. C: Struct. Chem.* **2015**, *71*, 3–8.
[79] G. M. Sheldrick, *SHELXT*: A programm for crystal structure solution, Vers. 2018/2012, University of Göttingen, Germany, **2018**.
[80] G. M. Sheldrick, *SHELXL*: A programm for crystal structure refinement, Vers. 2018/2013, University of Göttingen, Germany, **2018**.
[81] G. M. Sheldrick, *Acta Crystallogr., Sect. A: Fond. Adv.* **2008**, *64*, 112–122.
[82] Oxford Instruments, *AztecEnergy*, Vers. 3.1, Abingdon, UK, **2016**.
[83] G. J. Long, T. E. Cranshaw, G. Longworth, *Moessbauer Eff. Ref. Data J.* **1983**, *6*, 42–49.
[84] R. A. Brand, *WinNormos for Igor6*, Vers. for Igor 6.2 or above: 22/02/2017, University of Duisburg, Duisburg, Germany, **2017**.
[85] J. J. Yeh, I. Lindau, *At. Data Nucl. Data Tables* **1985**, *32*, 1–155.
[86] R. F. Reilmann, A. Msezane, S. T. Manson, *J. Electron. Spectrosc. Relat. Phenom.* **1976**, *8*, 389–394.
[87] S. Tanuma, C. J. Powell, D. R. Penn, *Surf. Interface Anal.* **1994**, *21*, 165–176.
[88] K. Schwarz, P. Blaha, G. K. Madsen, *Comput. Phys. Commun.* **2002**, *147*, 71–76.
[89] K. Schwarz, P. Blaha, *Comput. Mater. Sci.* **2003**, *28*, 259–273.
[90] J. P. Perdew, K. Burke, M. Ernzerhof, *Phys. Rev. Lett.* **1996**, *77*, 3865–3868.
[91] J. P. Perdew, K. Burke, M. Ernzerhof, *Phys. Rev. Lett.* **1997**, *78*, 1396.
[92] F. Tran, P. Blaha, *Phys. Rev. Lett.* **2009**, *102*, 226401.
[93] J. A. Camargo-Martínez, R. Baquero, *Phys. Rev. B* **2012**, *86*, 195106.
[94] K. Schwarz, A. Neckel, J. Nordgren, *J. Phys. F: Metal Phys.* **1979**, *9*, 2509–2521.
[95] J. McLeod, R. Green, E. Kurmaev, N. Kumada, A. Belik, A. Moewes, *Phys. Rev. B* **2012**, *85*, 195201.
[96] G. Mahan, *Phys. Rev. B* **1980**, *21*, 1421–1431.
[97] U. von Barth, G. Grossmann, *Phys. Rev. B* **1982**, *25*, 5150–5179.
[98] Bruker Optik GmbH, OPUS V8.7, Ettlingen, Germany, **2012**.
[99] W. H. Baur, A. A. Khan, *Acta Crystallogr., Sect. B: Struct. Sci., Cryst. Eng. Mater.* **1971**, *27*, 2133–2139.
[100] A. Huq, J. W. Richardson, E. R. Maxey, D. Chandra, E.-M. Chien, *J. Alloys Compd.* **2007**, *436*, 256–260.
[101] J. Hao, Y. W. Li, C. L. Ma, L. Y. Huang, R. Liu, Q. L. Cui, G. T. Zou, J. Liu, X. D. Li, *J. Phys. Chem. C* **2010**, *114*, 16750–16755.
[102] D. E. Partin, D. J. Williams, M. O'Keeffe, *J. Solid State Chem.* **1997**, *132*, 56–59.

Manuscript received: November 16, 2024
Accepted manuscript online: November 18, 2024
Version of record online: ■■, ■■

RESEARCH ARTICLE

Phase-pure, crystalline γ-Sn_3N_4 was synthesized via reaction of argon-diluted $SnCl_4$ with Mg_3N_2. The exothermic nature of the reaction is controlled by slow mixing of the starting materials with a continuous flow of argon. The reaction can be further facilitated by the use of a tin flux. This new method not only leads to pure γ-Sn_3N_4 material, but is also promising for the synthesis of other nitride materials.

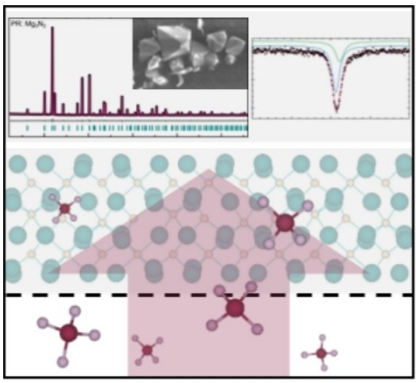

M. Zipkat, A. Koldemir, T. Block, C. Ceniza, T. D. Boyko, S. Kläger, R. M. Pritzl, A. Moewes, R. Pöttgen, S. S. Rudel, W. Schnick**